ARTICLE IN PRESS
EPSL:115909

Earth and Planetary Science Letters ••• (••••) ••••••

Contents lists available at ScienceDirect

Earth and Planetary Science Letters

www.elsevier.com/locate/epsl

D/H ratios and H_2O contents record degassing and rehydration history of rhyolitic magma and pyroclasts

Thomas Giachetti[a,*], Michael R. Hudak[a], Thomas Shea[b], Ilya N. Bindeman[a], Erin C. Hoxsie[a]

[a] *Department of Earth Sciences, University of Oregon, Eugene, OR, USA*
[b] *Department of Geology and Geophysics, University of Hawaii at Manoa, Honolulu, HI, USA*

ARTICLE INFO

Article history:
Received 3 July 2019
Received in revised form 14 October 2019
Accepted 15 October 2019
Available online xxxx
Editor: T.A. Mather

Keywords:
rehydration
pyroclastic obsidian
pumice
open-system degassing
closed-system degassing

ABSTRACT

Volcanic eruptions of rhyolitic magma often show shifts from powerful (Vulcanian to Plinian) explosive episodes to a more gentle effusion of viscous lava forming obsidian flows. Another prevailing characteristic of these eruptions is the presence of pyroclastic obsidians intermingled with the explosive tephra. This dense, juvenile product is similar to the tephra and obsidian flow in composition, but is generally less degassed than its flow counterpart. The formation mechanism(s) of pyroclastic obsidians and the information they can provide concerning the extent to which magma degassing modulates the eruptive style of rhyolitic eruptions are currently subject to active research. Porous tephra and pyroclastic and flow obsidians from the 1060CE Glass Mountain rhyolitic eruption at Medicine Lake Volcano (California) were analyzed for their porosity, ϕ, water content, H_2O, and hydrogen isotopic composition, δD. H_2O in porous pyroclasts is correlated negatively with δD and positively with ϕ, indicating that the samples were affected by post-eruptive rehydration. Numerical modeling suggests that this rehydration occurred at an average rate of $10^{-23.5\pm0.5}$ $m^2\,s^{-1}$ during the ~960 years since the eruption, causing some pyroclasts to gain up to 1 wt% of meteoric water. Pyroclastic and flow obsidians were not affected by rehydration due to their very low porosity. Comparison between modeled δD-H_2O relationships in degassing magma and values measured in the Glass Mountain samples supports the idea that rhyolitic magma degasses in closed-system until its porosity reaches a value of about 65±5%, beyond which degassing occurs in open-system until quench. During the explosive phase, rapidly ascending magma fragments soon after it becomes permeable, creating porous lapilli and ash that continue to degas in open-system within an expanding gas phase. As suggested by recent studies, some ash may aggregate and sinter on the conduit sides at different depths above the fragmentation level, partly equilibrating with the continuously fluxing heavier magmatic vapor, explaining the wide range of H_2O contents and high variability in δD measured in the pyroclastic obsidians. Using only H_2O and δD, it is impossible to rule out the possibility that pyroclastic obsidians may also form by permeable foam collapse, either syn-explosively near the conduit sides below the fragmentation level or during more effusive periods interspersed in the explosive phase. During the final effusive phase of the eruption, slowly ascending magma degasses in open-system until it reaches the surface, creating flows with low H_2O and δD. This study shows that H_2O measured in highly porous pyroclasts of a few hundred years or more cannot be used to infer syn-eruptive magma degassing pathways, unless careful assessment of post-eruptive rehydration is first carried out. If their mechanism of formation can be better understood, detailed analysis of the variations in texture and volatile content of pyroclastic obsidians throughout the explosive phase may help decipher the reasons why rhyolitic eruptions commonly shift from explosive to effusive phases.

1. Introduction

Volcanic eruptions of rhyolitic magma almost always undergo an overall transition from explosive to effusive activity during which powerful Vulcanian to Plinian phases precede the more gentle emplacement of thick obsidian flow(s)/dome(s). Examples include the 1340 CE eruption sequence at Mono Craters (California, USA, Newman et al., 1988), the 1300 BP eruption at Newberry Volcano (Oregon, USA, Rust and Cashman, 2007), the 1912 eruption at Novarupta (Alaska, USA, Hildreth and Fierstein, 2012), the 1060 CE eruption at Medicine Lake Volcano (California, USA, Heiken, 1978),

---

[*] Corresponding author.
E-mail address: tgiachet@uoregon.edu (T. Giachetti).

https://doi.org/10.1016/j.epsl.2019.115909
0012-821X/© 2019 Elsevier B.V. All rights reserved.

Please cite this article in press as: Giachetti, T., et al. D/H ratios and H_2O contents record degassing and rehydration history of rhyolitic magma and pyroclasts. Earth Planet. Sci. Lett. (2019), https://doi.org/10.1016/j.epsl.2019.115909

or the Chilean eruptions at Chaitén (2008, Lara, 2009) and Cordon Caulle (2011-2012, Silva Parejas et al., 2012), which are the only two witnessed rhyolitic eruptions reported to date. Because the hazards associated with each type of activity differ vastly, it is imperative to understand the timing of any explosive-effusive transition to appropriately mitigate the impact on populations and infrastructure during such events. Deposits of rhyolitic eruptions that have experienced shifts in their type of activity reveal a sharp transition between the explosive and the effusive phases. However, post-eruptive erosion and/or subsequent eruptions can overprint the stratigraphic signature of a relatively protracted explosive-effusive transition (i.e., occurring over weeks to months), and it is therefore crucial to rely on direct observations of such eruptions. For example, in the case of Cordon Caulle 2011-2012 eruption, it was witnessed that a single volcanic vent simultaneously produced rhyolitic lava effusion and (sub)-Plinian ash columns (Silva Parejas et al., 2012; Castro et al., 2013), and this hybrid explosive-effusive activity at a single vent might play a role in the overall transition from explosive to effusive activity (Schipper et al., 2013).

If obsidian domes/flows seem to invariably be the final product of all rhyolitic eruptions, fragments of juvenile obsidian are also consistently found in the tephra deposit that precede the final effusive phase (e.g., Newman et al., 1988; Rust and Cashman, 2007; Castro and Dingwell, 2009; Schipper et al., 2013). These mm-to-cm-size dense pyroclasts are a minor component of the tephra and often exhibit a wide range of textures and volatile contents (e.g., Taylor et al., 1983; Newman et al., 1988; Rust et al., 2004; Rust and Cashman, 2007), sometimes within the same clast (Gardner et al., 2017; Watkins et al., 2017). Their mode of formation and eruption remains an active area of research, with numerous postulated formation mechanisms. For example, pyroclastic obsidians have been thought to be unvesiculated pockets of melt (Newman et al., 1988), magma quenched by water within the conduit at aquifers level (Bursik, 1993), magma densified in a zone of high shear rates at conduit margins (Newman et al., 1988; Rust et al., 2004; Stasiuk et al., 1996), fragments of precursory dikes and/or glass-filled fractures (Rust and Cashman, 2007), or the result of repetitive melt fracturing and healing (Tuffen et al., 2003; Gonnermann and Manga, 2003; Cabrera et al., 2011; Castro et al., 2014). Based on textural observations, measurements of volatile content and numerical modeling of volatile diffusion in pyroclastic obsidians from the North Mono eruption, Gardner et al. (2017) and Watkins et al. (2017) recently proposed a new model in which pyroclastic obsidians form through multiple cycles of sintering of ash particles along conduit walls, followed by fracturing back into the eruptive column and ejection, all above the level of fragmentation.

To better constrain the origin and mode of formation of pyroclastic obsidians and the overall change in degassing style during rhyolitic eruptions that exhibit a change in type of activity with time, some studies have characterized the evolution of the texture and volatile content of pyroclastic obsidians throughout the explosive phase (Rust and Cashman, 2007), or compared the volatile content and hydrogen isotopic ratio of pyroclastic and flow obsidians with degassing models (Taylor et al., 1983; Newman et al., 1988; DeGroat-Nelson et al., 2001; Rust et al., 2004; Castro et al., 2014). In this study, we integrate numerical modeling of magma degassing with textural work, water contents and hydrogen isotope data obtained on the juvenile products of both the explosive (dense and porous tephra) and effusive (obsidian flow) phase of the 1060CE Glass Mountain eruption of Medicine Lake Volcano, California. Stratigraphic constraints on the samples allow us to track any systematics change in these parameters throughout the explosive phase. Numerical modeling of both syn-eruptive magma degassing and post-eruptive rehydration of the matrix glass was used to interpret our data. To this end, we assume different scenarios of magma ascent in the conduit and take into account relatively recent findings concerning the rehydration of porous samples by meteoric water (Giachetti and Gonnermann, 2013; Giachetti et al., 2015; Hudak and Bindeman, 2018), the onset of permeability development in expanding rhyolitic magma (Gonnermann et al., 2017; Giachetti et al., 2019), and test the recent model proposed for the formation of pyroclastic obsidians (Gardner et al., 2017; Watkins et al., 2017).

2. The 1060CE eruption of Medicine Lake Volcano and its products

The Glass Mountain eruption was the last event of the post-glacial eruptive activity of Medicine Lake Volcano (Anderson, 1933; Heiken, 1978; Donnelly-Nolan et al., 1990, 2008). The eruption consisted of a Plinian phase followed by the emplacement of rhyolite-dacite flows, with a total erupted volume of approximately 1 km^3 (Heiken, 1978). The Plinian phase produced a fallout deposit of 0.27 km^3 (Donnelly-Nolan et al., 2007), with no evidence for deposition by pyroclastic flows. New observations show that the proximal fallout deposits consist of multiple layers of relatively well sorted rhyolitic clasts. Most layers consist largely of pumices, with only a few thinner layers containing up to 60-80% of pyroclastic obsidians and lithics, distributed throughout the entire stratigraphic column, with a slightly higher frequency towards the base and top of the deposit. Most porous pyroclasts appear texturally homogeneous with <5% phenocrysts (Heiken, 1978), and approximately 3 vol% microlites (Stevenson et al., 1996). The chemical composition of the porous tephra and pyroclastic obsidians is similar to that of the Glass Mountain rhyolitic obsidian flow, with a SiO_2 content of 72-75 wt% (Anderson, 1933; Heiken, 1978; Grove and Donnelly-Nolan, 1986; Grove et al., 1997; Waters and Lange, 2016).

Melt inclusions and experimental petrologic studies indicate that the Glass Mountain rhyolitic magma formed under near H_2O-saturated conditions at pressures of 100-200 MPa (Grove et al., 1997), corresponding to ∼4-6 wt% of water assuming a temperature of 850 °C (Liu et al., 2005; Waters and Lange, 2016). Giachetti et al. (2015) calculated that highly porous fallout pumices contained 0.2-0.5 wt% of magmatic H_2O immediately after the eruption, gaining 1-2 wt% of water by rehydration, which is the diffusion of meteoric water in the matrix glass between the eruption and sample analysis. Tatlock et al. (1976), Taylor et al. (1983), DeGroat-Nelson et al. (2001) and Giachetti and Gonnermann (2013) measured 0.06-0.36 wt% of magmatic H_2O in the obsidian from the flow, while Taylor et al. (1983) obtained 0.41-1.93 wt% H_2O in pyroclastic obsidians found in the tephra deposit.

3. Methodology

3.1. Samples

Pyroclasts from the tephra deposit of the 1060CE Glass Mountain eruption were collected at 41.59°N and 121.51°W in a quarry about 2 km NNE of the hypothesized main vent for both the explosive and effusive phases. Thirty porous pyroclasts from the explosive phase of the Glass Mountain eruption were arbitrarily selected from a larger set of about 3,000 clasts collected across a complete 14-m-thick section of the fallout deposit. Additionally, at the same outcrop, we collected forty three pyroclastic obsidians from ten distinct layers rich in pyroclastic obsidians and lithics. Porous pyroclasts vary from 1.3 cm to 2.4 cm in size and do not show any obvious gradient in porosity or bubble size from center to margin. Although the least porous of these pyroclasts are almost completely dense, they do not exhibit the same glassy aspect as the pyroclastic obsidians and were therefore treated with the other porous pyroclasts. It should be noted that removing them

Please cite this article in press as: Giachetti, T., et al. D/H ratios and H_2O contents record degassing and rehydration history of rhyolitic magma and pyroclasts. Earth Planet. Sci. Lett. (2019), https://doi.org/10.1016/j.epsl.2019.115909

from the list of porous pyroclasts does not change our modeling results (Section 5) and conclusions. Pyroclastic obsidians are 0.5-2 cm in size and appear glassy with, in some cases, a color banding from black to dark gray (see microscope pictures in supplementary material). Additionally, three obsidian samples were collected on the southern edge of the Glass Mountain flow, on the flow surface. These samples were taken from meter-size blocks that appear glassy and relatively homogeneous in the field and collected a few centimeters away from the surface exposed to the atmosphere, to ensure that they were not affected by rehydration.

3.2. Porosity and bubble wall thickness distribution

The total porosity of the porous pyroclasts, ϕ, was determined using Archimede's principle, with an uncertainty of $<1\%$ (e.g., Houghton and Wilson, 1989; Shea et al., 2010). Observations of sections of some obsidians from the tephra and the flow using an optical microscope show that most of these samples are completely dense or have a bulk microporosity much lower than 5%. Samples from all three textural types were then finely crushed and the density of their solid phase was measured using a high precision balance and a helium pycnometer (e.g., Giachetti et al., 2010), resulting in a density of $\rho_s = 2.36 \pm 0.04$ g cm^{-3}, without any systematic variation between sample types. Scanning Electron Microscope (SEM) images of three porous pyroclasts covering a wide range of porosities (32.7%, 52.8%, and 74.9%) were taken at several total magnifications between 70× and 2000× to calculate the bubble wall thickness distribution (see Section 5). For each of the three samples, from 2,231 to 2,671 bubble walls at least 5 pixels thick (i.e., 0.18-0.30 µm depending on the sample) were highlighted on the SEM images, following Giachetti et al. (2015). Overlap between data from the different magnifications allowed for the calculation of the full bubble wall thickness distribution over the range $\sim 10^{-1}$-10^{2} µm.

3.3. Volatiles and δD

3.3.1. H_2O and δD

All powdered porous pyroclasts, flow obsidians and forty three pyroclastic obsidians were analyzed for total H_2O content and δD value at the Stable Isotope Laboratory at the University of Oregon on a MAT253 isotope ratio mass spectrometer (IRMS). Between 1.5 and 6 mg of powder, depending of water content, was loaded in Ag capsules, weighed, sealed and re-weighed to ensure no sample loss occurred during sealing of the capsule. The capsules were dried overnight at 130 °C in a vacuum oven to remove adsorbed water. A subset of samples were re-weighed once more after drying to ensure there was no significant mass loss related to adsorbed H_2O. Capsules were loaded into a high Temperature Conversion Elemental Analyzer (TC/EA) interfaced with the IRMS and dropped into a furnace lined with a glassy carbon tube at 1450 °C. Water vapor liberated from the melted samples at high temperatures undergoes a pyrolysis reaction with the glassy carbon to convert H_2O to H_2 and CO gas. The sample gas is passed through a gas chromatograph to the IRMS using a He carrier gas where pyrolyzed H_2 and CO are separated and H_2 is analyzed using an open split on a MAT253 mass spectrometer. During each analytical session, mica standards USGS57 (biotite) and USGS58 (muscovite, Qi et al., 2017) are analyzed 4-5 times each to calibrate both the total H_2O and δD data. Analytical error for δD is approximately ± 2‰ and water contents below 1.5 wt% have errors lower than ± 0.1 wt% (Martin et al., 2017). The isotopic results are expressed in a δD notation with respect to the V-SMOW standard, where $\delta D = (R/R_{\text{V-SMOW}} - 1) \times 10^3$ and R is the D/H isotopic ratio of the sample. As the crystal content in the samples is <5% and minerals present are anhydrous (Heiken, 1978; Stevenson et al., 1996), we assume that the values obtained are similar to what would be obtained for the matrix glass only.

Table 1
H_2O content and deuterium/hydrogen isotopic ratio, both obtained by TC/EA on pyroclastic obsidians and obsidians from Glass Mountain flows (gray cells).

Sample	H_2O (wt%)	δD (‰)
LR-L-1-2	0.83	−81
LR-L-1-3	0.76	−80
LR-L-1-4	1.08	−82
LR-L-1-5	0.97	−103
LR-L-1-6	0.61	−81
LR-L-2-1	0.72	−87
LR-L-2-4	0.69	−106
LR-L-2-3	0.1	−98
LR-L-3-1	0.28	−107
LR-L-3-2	0.72	−92
LR-L-3-3	0.53	−94
LR-L-3-4	1.16	−75
LR-L-3-5	0.79	−85
LR-L-4-5	0.77	−83
LR-L-4-2	0.58	−85
LR-L-4-7	0.6	−85
LR-L-4-6	0.63	−104
LR-L-4-1	0.69	−91
LR-L-4-3	0.82	−92
LR-L-5-1	0.59	−93
LR-L-6-1	0.95	−87
LR-L-6-2	0.49	−96
LR-L-6-3	0.16	−104
LR-L-6-5	0.46	−94
LR-L-7-1	0.48	−103
LR-L-7-3	0.07	−90
LR-L-9-1	0.69	−81
LR-L-9-2	0.77	−81
LR-L-9-3	0.6	−93
LR-L-9-4	0.7	−84
LR-L-9-5	0.91	−91
LR-L-9-6	0.32	−91
LR-L-9-7	0.08	−85
LR-L-10-1	0.4	−77
LR-L-10-2	1.04	−83
LR-L-10-4	0.76	−91
LR-L-10-6	1.58	−65
LR-L-10-7	0.64	−88
LR-L-10-8	0.77	−80
LR-L-12-1	0.32	−95
LR-L-12-2	0.53	−81
LR-L-12-3	0.36	−91
Sample	H_2O (wt%)	δD (‰)
Obs1	0.44	−99
Obs2	0.25	−100
Obs3	0.25	−105

3.3.2. H_2O speciation and CO_2

Five pyroclastic obsidians were analyzed by Fourier Transform InfraRed spectroscopy (FTIR) to quantify water speciation and CO_2 content. Measurements of hydroxyl water (OH), molecular water (H_2O_m), and CO_2 concentrations were made using a Thermo Nicolet Nexus 670 FTIR spectrometer at the University of Oregon on 220-403-µm-thick double-polished slices of the samples. Wafer thickness was measured using a digital micrometer with a 1 µm precision. Absorbance was obtained using a 15× objective, infrared source, MCT-A detector, and KBr beamsplitter. Measurements were made along a single 2.4 mm to 5.2 mm long profile in each sample, collecting 64 scans per spot every 100 µm and using an aperture of 100 µm and a spectral resolution of 4 cm^{-1}. Contents of OH and H_2O_m were determined from absorbances at 4500 cm^{-1} and 1630 cm^{-1}, respectively, using the Beer-Lambert law and absorption coefficients of 1.73 ± 0.02 L cm^{-1} mol^{-1} and 55 ± 2 L cm^{-1} mol^{-1}, respectively (Newman et al., 1986). Conversion of absorbance at 2350 cm^{-1} to concentration of CO_2 was made using an absorption coefficient of 1214 ± 78 L cm^{-1} mol^{-1} (Behrens et al., 2004). Only average value and standard deviation along the profile are provided here. Raw absorbance profiles at 1630, 2350, 3550, 4500, and 5230 cm^{-1} and sample thicknesses are provided in Supplementary material.

4. Results

4.1. Obsidians

Pyroclastic obsidian water contents obtained by TC/EA are in the range 0.07-1.58 wt% (Table 1), with an average of 0.66 ± 0.31 wt%, varying widely by 0.5-1 wt% within individual layers (Fig. 1a). Additionally, more than 90% of the pyroclastic obsidians analyzed have a water content lower than 1 wt%. Water contents measured by FTIR are in agreement with these values, with H_2O contents

Please cite this article in press as: Giachetti, T., et al. D/H ratios and H_2O contents record degassing and rehydration history of rhyolitic magma and pyroclasts. Earth Planet. Sci. Lett. (2019), https://doi.org/10.1016/j.epsl.2019.115909

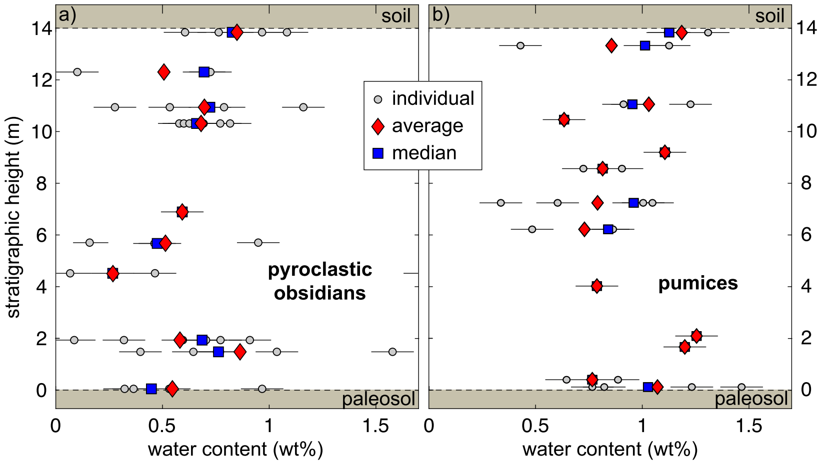

Fig. 1. Water content of a) pyroclastic obsidians and b) porous pyroclasts measured by TC/EA as a function of their stratigraphic height above the paleosol. From one to six individual clasts were analyzed for each layer in the stratigraphy, and both the average and median water contents are shown, in addition to individual values.

Table 2
Water and CO_2contents obtained by FTIR on selected pyroclastic obsidians. Temperature, T, is calculated using speciation and the model of Zhang et al. (1997). Pressure is then obtained using the model of Liu et al. (2005) and calculated T. Values correspond to the average and standard deviation along a 2.4-5.2-mm profile. For CO_2 data, the value in parentheses corresponds to maximum amount measured along the profile.

Sample	H_2O (wt%)	H_2O_m (wt%)	OH (wt%)	CO_2 (ppm)	T (°C)	P (MPa)
LR-L-1-4	0.47±0.03	0.10±0.01	0.37±0.02	1±4 (8)	472±17	1.0±0.1
LR-L-2-2	0.69±0.13	0.18±0.06	0.51±0.06	1±5 (15)	490±41	2.2±0.3
LR-L-4-4	0.57±0.11	0.17±0.01	0.40±0.10	0±5 (11)	420±77	1.3±0.4
LR-L-7-2	0.47±0.03	0.06±0.01	0.41±0.02	0±3 (5)	635±34	1.4±0.1
LR-L-10-2	0.58±0.06	0.13±0.01	0.45±0.05	3±8 (27)	502±50	1.6±0.3

in the range 0.47-0.69 wt% and an average of 0.56±0.09 wt% (Table 2). FTIR measurements in pyroclastic obsidians also show that 70-88% of the water, in terms of mass, consist of hydroxyl groups, and that $CO_2 < 15$ ppm, except for a peak at 27 ppm in one sample. Fig. 1a shows that there is no strong relationships between the water content of a pyroclastic obsidian and its relative position in the stratigraphy, although the average/median water content within a layer seems to gradually increase in the upper two-thirds of the deposit, from ∼0.4 wt% at 4.5 meters above the paleosol to ∼0.9 wt% towards the top of the tephra deposit. The δD in the pyroclastic obsidians varies from −106.8‰ to −64.5‰ with an average of −88±9‰, and is roughly positively correlated with water content (Fig. 2). These values are essentially consistent with those of Taylor et al. (1983) obtained on pyroclastic obsidians from the same eruption. They measured 0.41-1.93 wt% H_2O and $\delta D = -74\pm11$‰ and also observed a positive correlation between H_2O and δD.

Water contents in the flow obsidians are in the range 0.25-0.44 wt% and $\delta D = -101\pm3$‰ (Table 1). These water contents are consistent with those of Giachetti and Gonnermann (2013) (0.24-0.36 wt%) and Tatlock et al. (1976) (0.11-0.35 wt%) obtained on similar samples but with different techniques. Data obtained by Taylor et al. (1983) show that their flow obsidians were slightly more degassed with lower H_2O contents in the range 0.12-0.26 wt% and lower δD of −124±7‰. DeGroat-Nelson et al. (2001) measured even lower H_2O contents of 0.06-0.14 wt% and δD of −136±11‰ in the Glass Mountain flow obsidians. Because our flow obsidians were collected several centimeters below the surface of the block in contact with the atmosphere, these samples are not affected by post-eruptive rehydration and the variability in H_2O contents between these five datasets may simply reflect the heterogeneity in water content of the obsidian flows.

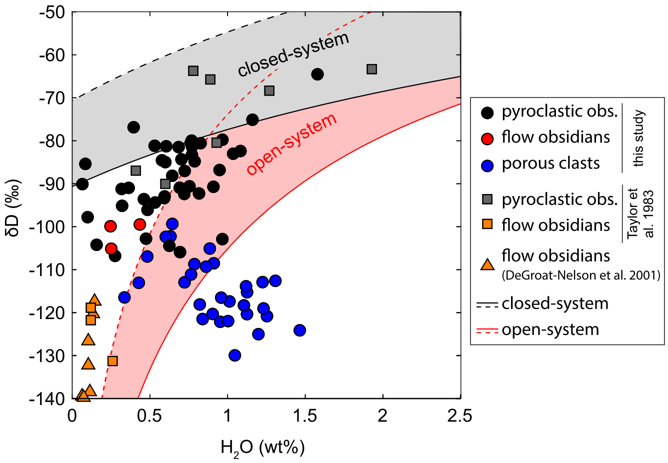

Fig. 2. Hydrogen isotopic ratios as a function of water content of obsidians from the rhyolitic flow, and obsidians and porous pyroclasts from the explosive phase of the Glass Mountain eruption (samples from this study and from that of Taylor et al. (1983) and DeGroat-Nelson et al. (2001)) and degassing models assuming pure closed- (gray area) or open-system (red area) degassing with an initial magmatic water content of 4 wt% (dashed line) or 6 wt% (solid line) and an initial δD of −50‰ to −30‰. (For interpretation of the colors in the figure(s), the reader is referred to the web version of this article.)

4.2. Porous pyroclasts

The water contents of the porous pyroclasts vary from 0.34 wt% to 1.47 wt% and is not correlated with the stratigraphic height of the sample (Table 3, Fig. 1). It is, however, strongly correlated with pyroclast porosity, which varies from 3.4% to 87.4% (Fig. 3). The D/H isotopic ratios range from −130‰ to −99‰ and is negatively correlated with both the water content and the porosity (Fig. 2). Measured bubble wall thicknesses vary from 0.9 μm to

Please cite this article in press as: Giachetti, T., et al. D/H ratios and H_2O contents record degassing and rehydration history of rhyolitic magma and pyroclasts. Earth Planet. Sci. Lett. (2019), https://doi.org/10.1016/j.epsl.2019.115909

Table 3
Water content (H_2O), isotopic ratio (δD), solid phase density (ρ_s), and porosity obtained on porous pyroclasts.

Sample	H_2O (wt%)	δD (‰)	ρ_s ($g\,cm^{-3}$)	Porosity (%)
L1-27	1.13	−115	2.36	75.5
L1-30	1.31	−113	–	84.3
L1-47	1.12	−114	2.37	43.5
L2-45	1.13	−120	2.45	87.4
L2-47	1.01	−117	2.35	87.0
L2-73	0.43	−113	2.52	11.8
L4-11	0.91	−108	2.26	49.4
L4-35	1.23	−113	2.25	76.4
L4-84	0.95	−122	2.31	66.0
L6-72	0.63	−102	2.39	21.3
L9-82	1.11	−118	2.36	52.5
L10-84	0.72	−113	2.37	34.9
L10-100	0.90	−120	–	68.6
L12-61	0.34	−116	2.41	3.4
L12-65	1.05	−130	2.39	80.0
L12-72	1.00	−122	2.34	65.8
L12-86	0.60	−102	2.38	14.2
L12-88	0.96	−116	2.38	45.0
L15-17	0.48	−107	2.35	26.5
L15-48	0.84	−121	2.32	60.8
L15-83	0.86	−109	2.36	26.3
L19-82	0.79	−109	2.35	40.2
L24-59	1.25	−121	2.34	84.9
L25-15	1.20	−125	2.38	86.6
L27-31	0.64	−99	2.32	58.3
L27-88	0.89	−105	2.31	61.6
L28-48	1.23	−119	2.33	72.9
L28-55	0.77	−111	2.38	36.3
L28-58	0.82	−118	2.33	42.7
L28-85	1.47	−124	2.53	84.2

45 µm and the distributions of wall thicknesses all show a single mode at about 9 µm for the most porous sample to 16 µm for the densest one. The bubble wall distribution, in volume terms, shows roughly the characteristic symmetric bell curve of a Gaussian function, with an expected value that decreases and a variance that increases with increasing porosity (Fig. 4). These distributions were fitted using a single-peak Gaussian model of the fit function in MATLAB®. The volume fraction, X_L, occupied by bubble walls of half thickness L is obtained by

$$X_L = a \times \exp\left(-\left[\frac{\log(L) - b}{c}\right]^2\right), \tag{1}$$

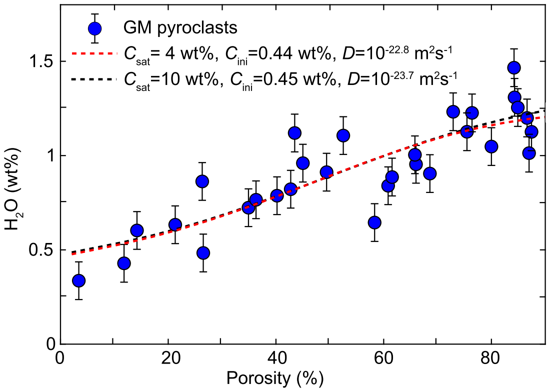

Fig. 3. Water content of the pyroclasts as a function of their porosity and best fits of the rehydration model obtained for $C_{sat} = 4$ wt% (dashed red line) and $C_{sat} = 10$ wt% (dashed black line). (For interpretation of the colors in the figure(s), the reader is referred to the web version of this article.)

where

$$a = -0.090\phi^2 + 0.033\phi + 0.143, \tag{2}$$

$$b = 1.178\phi^2 - 1.890\phi + 1.405 \tag{3}$$

and

$$c = 0.576\phi^2 - 0.390\phi + 0.459. \tag{4}$$

Here L is expressed in µm and a, b, and c are empirical factors that are found to solely depend on the porosity of the sample, ϕ, expressed in volume fraction.

5. Modeling porous pyroclasts rehydration

5.1. ϕ-H_2O relationships

The meteoric origin of most of the water present in the porous pyroclasts is corroborated by both the anti-correlation between water content and δD (Fig. 2) and the positive correlation between H_2O and ϕ (Fig. 3). Pumices with thinner bubble walls are more rehydrated than the denser ones because of a higher surface area over volume ratio (e.g., Giachetti and Gonnermann, 2013; Giachetti et al., 2015; Seligman et al., 2016). We carried out numerical modeling of glass hydration to test whether this observation can

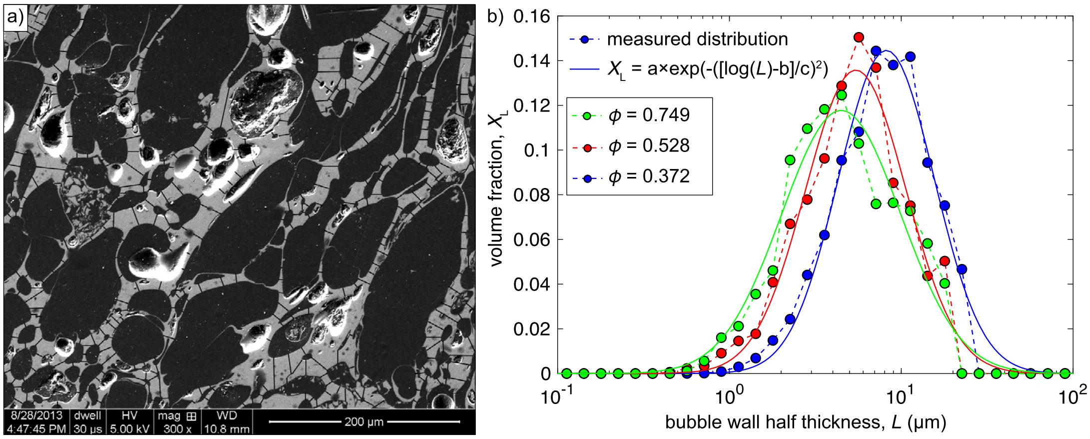

Fig. 4. Bubble wall distribution. a) Scanning Electron Microscope image of a pumice with a porosity of 74.9%. Each black line represents the measurement of one bubble wall thickness (2,231-2,671 measured per sample). b) Bubble wall half thickness distribution, in volume fraction, X_L, and assuming spherical shape, for three samples with a wide range of porosities. Distributions are fitted using $X_L = a \times \exp(-([\log(L) - b]/c)^2)$, where X_L is the volume fraction of bubble walls with a half thickness of L, and a, b, and c are empirical coefficients that solely depend on porosity.

Please cite this article in press as: Giachetti, T., et al. D/H ratios and H_2O contents record degassing and rehydration history of rhyolitic magma and pyroclasts. Earth Planet. Sci. Lett. (2019), https://doi.org/10.1016/j.epsl.2019.115909

be solely explained by post-eruptive diffusion of water into the glass at atmospheric surface temperature during the approximately 960 years between pyroclast deposition and analysis. Most of the vesicles in the Glass Mountain pyroclasts are interconnected (cf., Gonnermann et al., 2017). As a result, it is expected that there is sufficient moisture at any time at the vesicle/glass interface for water to diffuse from the vesicle-glass interface into the matrix glass (e.g. Ross and Smith, 1955; Friedman and Smith, 1958; Friedman and Long, 1976; Newman et al., 1986; Tuffen et al., 2010).

In the model, we assume a spherical geometry and a homogeneous distribution of vesicles with an average bubble radius, R, that depends on the porosity, ϕ, and bubble number density, N, following

$$R=\left(\frac{3}{4\pi}\frac{\phi}{N(1-\phi)}\right)^{1/3}. \tag{5}$$

The bubble number density is taken constant and equal to 4×10^{14} m^{-3} of melt for all the samples (Gonnermann et al., 2017). Water diffuses from R towards $R+L$ where L is the bubble wall half thickness, which covers a wide range of sizes inside each sample and whose distribution varies from sample to sample (Section 4.2).

With time, the water content in the matrix glass increases due to diffusion of meteoric water following

$$\frac{\partial c}{\partial t}=D\left(\frac{\partial^2 c}{\partial r^2}+\frac{2}{r}\frac{\partial c}{\partial r}\right). \tag{6}$$

Here t (s) is the time, $c(r,t)$ is the water concentration in the matrix glass in wt%, r (m) is the radial coordinate, and D is the diffusivity of water in rhyolitic glass at rehydration conditions expressed in $m^2\,s^{-1}$. The initial and boundaries conditions are

$$c=C_{\mathrm{ini}}\quad \text{at}\quad R\le r\le R+L\quad\text{and}\quad t=0, \tag{7}$$

$$\left(\frac{\partial c}{\partial t}\right)_{r=R+L}=0\quad\text{at}\quad t\ge 0, \tag{8}$$

$$c=C_{\mathrm{sat}}\quad\text{at}\quad r=R+L\quad\text{and}\quad t>0. \tag{9}$$

The volumetrically averaged concentration of water in the matrix glass, C_{m_L}, is calculated at $t=960$ years for thirty bubble wall half thicknesses between 0.1 and 100 μm (from $\log[L]=-1$ to $\log[L]=2$ by increment of 0.1). The average water content in the sample is equal to

$$C_{\mathrm{m}}=\sum_{L=10^{-1}}^{10^2}X_{\mathrm{L}}C_{m_L}, \tag{10}$$

where X_{L} is the volumetric fraction of bubble walls of half thickness L, which is obtained using Equations (1)-(4) and for L from 0.1 to 100 μm.

The numerical modeling could account for variable C_{ini} depending on sample porosity (for example), but in the absence of evidence to strengthen such hypothesis it was decided to take C_{ini} equal for all samples, and C_{ini} is allowed to vary within the range $0-2$ wt%. The boundary condition C_{sat} corresponds to the solubility of water at atmospheric pressure and temperature, which is poorly constrained (e.g., see discussion in Giachetti and Gonnermann, 2013). We therefore arbitrarily allow C_{sat} to vary between 2 wt% and 10 wt%. Finally, the diffusivity of water in rhyolitic glass at atmospheric conditions is also poorly constrained as values reported in the literature vary by orders of magnitude in the range $10^{-24.1}-10^{-20.7}$ $m^2\,s^{-1}$ (e.g., Friedman and Smith, 1960; Friedman and Long, 1976; Liritzis et al., 2004; Giachetti and Gonnermann, 2013; Rempel and Bindeman, 2019, and references therein). In the model, D is allowed to vary within the aforementioned range. We then research the values of C_{ini}, C_{sat}, and D that minimize (non-weighted least squares) the root-mean-square error (RMSE) between measured and predicted water concentrations. It is found that the RMSE is correlated with C_{sat} following a power law of the form

$$\mathrm{RMSE}=0.0229\times C_{\mathrm{sat}}^{-2.679}+0.144, \tag{11}$$

with D and C_{ini} both correlated with C_{sat} following power law relationships respectively of the form

$$\log(D)=5.28\times C_{\mathrm{sat}}^{-0.3393}-26.16, \tag{12}$$

and

$$C_{\mathrm{ini}}=-0.35\times C_{\mathrm{sat}}^{-2.413}+0.45. \tag{13}$$

In Equations (11)-(13), C_{sat} and C_{ini} are both expressed in wt% and D in $m^2\,s^{-1}$. The data can be reasonably well fitted by the model for any value of C_{sat} in the range 4-10 wt%, giving $C_{\mathrm{ini}}=0.45\pm0.01$ wt% and $D=10^{-23.3\pm0.5}$ $m^2\,s^{-1}$ (Fig. 3). The amount of magmatic water, $C_{\mathrm{ini}}=0.45$ wt%, is consistent with the range 0.2-0.5 wt% given by Giachetti et al. (2015) for similar samples from the Glass Mountain eruption and with the general idea that silicic pyroclasts from highly explosive eruptions are largely degassed when deposited (e.g., Gerlach et al., 1996; Castro et al., 2014). The diffusivity is here constrained within an order of magnitude at $10^{-23.3\pm0.5}$ $m^2\,s^{-1}$, a range that includes the value found by Giachetti and Gonnermann (2013) for the same eruption ($10^{-23.8}$ $m^2\,s^{-1}$), and is rather consistent with the value obtained by extrapolating to 25 °C the model of water diffusivity of Zhang and Ni (2010) valid for temperatures >400 °C ($10^{-24.2}$ to $10^{-23.4}$ $m^2\,s^{-1}$, assuming a water content of 0.5-1 wt%).

5.2. H_2O-δD relationships

The δD of rehydrating pyroclasts is given by (Seligman et al., 2016)

$$\delta\mathrm{D}=F_{\mathrm{met}}(\delta\mathrm{D}_{\mathrm{met}}-\Delta_{\mathrm{glass-met}})+(1-F_{\mathrm{met}})\delta\mathrm{D}_{\mathrm{glass}}, \tag{14}$$

where F_{met} is the fraction by weight of water in glass that is meteoric, $\delta\mathrm{D}_{\mathrm{met}}$ is the δD of the local meteoric water, $\Delta_{\mathrm{glass-met}}=10^3\ln(\alpha_{\mathrm{glass-met}})\approx-33‰$ is the fractionation factor between the meteoric water and the glass (Friedman et al., 1993; Seligman et al., 2016), and $\delta\mathrm{D}_{\mathrm{glass}}$ is the δD of the sample before rehydration. Meteoric water in the Medicine Lake Volcano area has a current annual mean $\delta\mathrm{D}_{\mathrm{met}}$ of −92‰ to −98‰ (Taylor et al., 1983; Davisson and Rose, 1997; Bowen et al., 2005). A value of −95‰ was used in our model, assuming δD did not vary much for the last thousand years. This assumption is supported by Mandeville et al. (2009) who found that glass rehydration at Crater Lake (7700 BP), which is located less than 160 km north of Medicine Lake Volcano, records values consistent with modern meteoric water, showing that there was probably little variation of the climate in the region after the end of the last deglaciation. Fig. 6 shows that the values of δD and H_2O measured in the porous pyroclasts can be explained by the rehydration of pyroclasts over about a thousand years with an initial water content of approximately 0.45 wt% and initial δD of −100±15‰ (see Section 6). Note that reclassifying the clasts with the lowest porosities as 'pyroclastic obsidians' rather than 'porous pyroclasts' does not change these results.

5.3. Implications and future directions

Our numerical models of water diffusion and isotopic exchange in porous pyroclasts after the eruption show once again that very

Please cite this article in press as: Giachetti, T., et al. D/H ratios and H_2O contents record degassing and rehydration history of rhyolitic magma and pyroclasts. Earth Planet. Sci. Lett. (2019), https://doi.org/10.1016/j.epsl.2019.115909

careful steps must be taken while interpreting raw water contents and isotopic compositions obtained on porous pyroclasts. In our case, the powdered samples were kept under vacuum at 130 °C overnight to remove adsorbed water, and such sample preparation is not sufficient to remove secondary water from the sample matrix glass. Because both water solubility and diffusivity at atmospheric conditions in rhyolitic glass are not well constrained, it is currently difficult to use numerical model of rehydration to estimate the exact amount of secondary water in pumices and resolve any potential relationships between magmatic water and porosity inherited from pre- and syn-eruptive magma degassing.

Several directions are conceivable to either tackle or circumvent this problem. Using Infrared or Raman spectroscopy at discrete locations away from any vesicles to avoid rehydrated areas might be a solution to measure matrix glass water content. However, it is always extremely challenging to find areas large enough (and also thick enough in the case of transmission FTIR) in highly porous pyroclasts to apply these techniques (McIntosh et al., 2017; Mitchell et al., 2018). Moreover, unless profiles of water content perpendicular to vesicle walls are carried out, such discrete analyses will not resolve the last diffusion behavior of the clast before the magmatic water content gets locked in (i.e., degassing, 'regassing', equilibrium; Watkins et al., 2012; McIntosh et al., 2014). Another approach would be to better constrain water solubility and diffusivity in rhyolitic glass at atmospheric conditions. The major challenge here is experimental and analytical as low temperature rehydration experiments are rather long and create only microns long diffusion profiles that are difficult to measure precisely on many experimental samples (see Anovitz et al., 2009; Liritzis and Laskaris, 2011, and references therein). Plus, water diffusivity presumably increases with increasing total water content (i.e., with time in the case of rehydration), calling for large sets of experiments to be able to resolve this dependency.

6. Modeling magma degassing

The results of our rehydration model suggest that diffusion of secondary water into the matrix-glass of the Glass Mountain products occurred at an average rate of $10^{-23.3\pm0.5}$ $m^2\,s^{-1}$ (Section 5.1), corresponding to a rehydrated layer of about 0.45±0.25 μm in 960 years. The size of the smallest pyroclastic obsidian analyzed is ~0.5 cm. Assuming it is spherical, the presence of a 0.45-μm-thick rehydrated layer with a (meteoric) water content of 5 wt% all around the pyroclastic obsidian represents an increase in water content of 0.003 wt%, which is well below the analytical error of both FTIR and TC/EA. The water content measured in pyroclastic obsidians (and in the obsidians from the flow collected few centimeters below the surface exposed to the atmosphere) therefore represents magmatic water only. In this section, we investigate different scenarios of syn-eruptive magma degassing to explain the magmatic water contents and hydrogen isotopic ratios measured in these samples.

6.1. Description of the model

6.1.1. Governing equations

In silicate melts, water dissolves as both molecular water, H_2O_m, and hydroxyl groups, OH (Stolper, 1982). The much higher diffusivity of H_2O_m compared to OH leads to variations in the water speciation during magma degassing. Because hydrogen is preferentially retained in the non-diffusive hydroxyl groups in the melt, hydrogen isotope compositions are also sensitive to magma degassing and subtle to extreme D/H fractionation occurs in response to both progressive closed- and open-system degassing, respectively (Taylor et al., 1983). The δD-H_2O relationships observed in pyroclastic and flow obsidians are the result of this isotopic partitioning during magma degassing (whereas, as shown in Section 5.2, the δD-H_2O relationships observed in pumices are inherited from post-eruptive rehydration by meteoric water). It is possible to test which degassing mechanisms prevail during the ascent of silicic magma by modeling the theoretical δD-H_2O path followed by ascending magma and comparing the resultant trajectories with that formed by values measured in the pyroclastic and flow obsidians (e.g., Taylor et al., 1983; Newman et al., 1988; Harford et al., 2003; Rust et al., 2004; Castro et al., 2014). To determine this degassing path, several configurations have been tested: 'pure' closed- or open-system degassing (Taylor et al., 1983; Newman et al., 1988; Castro et al., 2014), two-stage degassing (i.e., closed-system degassing followed by open-system; e.g., Kusakabe et al., 1999; Rust et al., 2004), or multiple steps of closed- and open-system degassing (Taylor, 1991; Castro et al., 2014). Buffering of degassing by continual flux of vapor through highly permeable, brecciated magma along conduit walls has also been considered (Rust et al., 2004).

In a closed-system, exsolved fluids remain in contact with the melt and both continuously equilibrate during ascent. In these conditions, the final D/H isotopic ratio of the H_2O in the pyroclast, R_f, is obtained by mass balance using (e.g., Taylor, 1991; Harford et al., 2003)

$$R_f = R_i - (1 - F)\ln\alpha_{v-m}, \tag{15}$$

where R_i is the initial D/H isotopic ratio of the melt or pyroclast, F is the fraction of H_2O remaining in the melt (i.e., concentration of H_2O at the pressure drop divided by initial H_2O concentration that is fixed and equal to the original magmatic value), and α_{v-m} is the hydrous speciation-dependent bulk H-isotope fractionation factor between hydrous vapor and rhyolite melt. δD (in ‰) is then calculated from R_f as described in Section 3.3.1. Even for a decrease in H_2O of several wt%, the decrease in δD is relatively modest in a closed-system, few ‰ to few tens of ‰ at most. Conversely, in an open-system, the instantaneous and continuous removal of the exsolved volatiles from the melt prevents isotopic equilibration between exsolved and dissolved H_2O, therefore leading to greater D/H fractionation. Open-system degassing (Rayleigh fractionation), is modeled by (e.g., Taylor, 1991; Harford et al., 2003)

$$R_f = R_i \times F^{\alpha_{v-m}-1}. \tag{16}$$

In both open and closed system degassing, the coexisting vapor produced has an isotopic ratio given by

$$R_v = \alpha_{v-m} \times R_i \times F^{\alpha_{v-m}}, \tag{17}$$

whereas the isotopic ratio of the accumulated vapor phase since the magma started to degas is given by

$$R_v^{acc} = \frac{F^{\alpha_{v-m}} - 1}{F - 1} \times R_i. \tag{18}$$

6.1.2. Fractionation factor between water vapor and melt

Water dissolves as both H_2O_m and OH in silicate melts and the hydrogen isotope fractionation between these two species and water vapor is different (e.g., Newman et al., 1988; Dobson et al., 1989; Taylor, 1991; Kusakabe et al., 1999). As a consequence, the bulk fractionation factor between water vapor and the coexisting melt, α_{v-m}, varies with water speciation and thus with water content during magma degassing. It can be calculated using (Newman et al., 1988; Dobson et al., 1989)

$$\alpha_{v-m} = \frac{X_{H_2O_m}}{X_{H_2O_t}} \times \alpha_{v-H_2O_m(melt)} + \left(1 - \frac{X_{H_2O_m}}{X_{H_2O_t}}\right) \times \alpha_{v-OH(melt)},$$

Please cite this article in press as: Giachetti, T., et al. D/H ratios and H_2O contents record degassing and rehydration history of rhyolitic magma and pyroclasts. Earth Planet. Sci. Lett. (2019), https://doi.org/10.1016/j.epsl.2019.115909

$$(19)$$

where $X_{H_2O_m}/X_{H_2O_t}$ and $1-(X_{H_2O_m}/X_{H_2O_t})$ are the mole fractions in the melt on a single-oxygen basis of H_2O as molecular water and hydroxyl groups, respectively. These can be calculated using (Zhang, 1999; Zhang and Ni, 2010)

$$X_{H_2O_t} = \frac{\dfrac{C_{H_2O_t}}{18.0152}}{\dfrac{C_{H_2O_t}}{18.0152} + \dfrac{100 - C_{H_2O_t}}{W}} \tag{20}$$

and

$$X_{H_2O_m} = \frac{8X^2_{H_2O_t}}{K(1-2X_{H_2O_t}) + 8X_{H_2O_t} + \sqrt{K^2(1-2X_{H_2O_t})^2 + 16KX_{H_2O_t}(1-X_{H_2O_t})}}. \tag{21}$$

Here $C_{H_2O_t}$ (wt%) is the concentration of total water in the melt (glass), $W = 32.49\ \mathrm{g\,mol^{-1}}$ is the composition-dependent molar mass of the dry melt per mole of oxygen (see Zhang and Ni, 2010, and references therein), and K is the equilibrium constant of the speciation reaction, $K = X^2_{OH}/(X_{H_2O_m}X_O)$. The equilibrium water speciation in rhyolitic melt has been extensively investigated over the last decades (e.g., Newman et al., 1986; Zhang et al., 1997; Nowak and Behrens, 2001; Hui et al., 2008; Zhang and Ni, 2010, and references therein) and a frequently used speciation model is given by (Zhang et al., 1997)

$$K = \exp\left(1.876 - \frac{3110}{T}\right), \tag{22}$$

where T (K) is the temperature. Comparing the results obtained using two different speciation models (Zhang et al., 1997; Nowak and Behrens, 2001), shows that the model results are little affected by the speciation model used (Fig. A.1a).

Experiments by Dobson et al. (1989) have shown that at 850 °C and $C_{H_2O_t} \approx 0.16$ wt%, the bulk fractionation factor between water vapor and the coexisting melt is 1.041. Under these conditions, speciation models show that about 99% of the water is in the OH form and it is therefore reasonable to assume that $\alpha_{v-OH(melt)} = 1.041$. At 950 °C and $C_{H_2O_t} = 3.1$ wt%, Taylor (1986) estimated that the bulk fractionation factor between water vapor and the coexisting melt is $\alpha_{v-m} = 1.024$. Under these conditions and using Equations (20)-(21), $X_{H_2O_m}/X_{H_2O_t} \approx 0.29$. Assuming $\alpha_{v-OH(melt)} = 1.041$ is constant and $\alpha_{v-m} = 1.024$, Equation (19) gives $\alpha_{v-H_2O_m(melt)} = 0.982$. It is thus possible to calculate the equilibrium constant K using Equation (22) assuming T is known and, for a given total amount of water $C_{H_2O_t}$, to calculate $X_{H_2O_m}$ and $X_{H_2O_t}$ using Equations (20) and (21), and finally α_{v-m} via Equation (19). For $T = 850$ °C, α_{v-m} increases from 1.019 for $C_{H_2O_t} = 5$ wt% up to 1.041 for $C_{H_2O_t} = 0.1$ wt%, when most of the magmatic water is in the OH form.

6.1.3. Initial conditions

Grove et al. (1997) showed that Glass Mountain magma was stored near H_2O-saturated conditions at pressures of 100-200 MPa, which corresponds to about 4-6 wt% of water assuming a temperature of about 850 °C (Liu et al., 2005; Waters and Lange, 2016). We therefore used an initial value of 5±1 wt% for $C_{H_2O_t}$ in our degassing models. For the δD of the parental undegassed magma, Taylor et al. (1983) chose a δD_i of −65‰, corresponding to the highest δD value measured in pyroclastic obsidians from Little Glass Mountain (for a $C_{H_2O_t}$ of 3.1 wt%), which is an eruption at Medicine Lake very similar to that of Glass Mountain (e.g., Heiken, 1978; Taylor et al., 1983). Similarly, our highest δD value is −65‰, measured in the most water-rich pyroclastic obsidian (1.58 wt%, see Table 1). However, using $\delta D_i = -65$‰ implies that the pyroclastic obsidian with 1.58 wt% did not degas, which is unrealistic as initial $C_{H_2O_t} = 4-6$ wt% (Grove et al., 1997). Instead, we chose an initial δD_i of −40±10‰, a range that encompasses most of the values provided in the literature for subduction magmas (e.g., Taylor, 1986; Seligman et al., 2016; Martin et al., 2017, and references therein). The sensitivity of the model to the initial δD and water content is illustrated in Figs. A.1b and c, respectively.

6.2. Model results and discussion

6.2.1. Degassing style

Fig. 2 shows that only 20% of the pyroclastic obsidians can be explained by degassing in ‘pure’ closed-system of a magma with an initial water content of 5±1 wt% and a δD_i of −40±10‰. Similarly, ‘pure’ open-system degassing of the same initial magma can account for only 40% of the measurements made on pyroclastic obsidians, and also fails to explain the relatively high δD of the obsidians from the flow. The degassing path followed by pyroclastic obsidians and obsidians from the flow must therefore be more complex.

Recent studies have shown that, during its ascent to the surface, rhyolitic magma becomes permeable when its porosity reaches about 60-70% (i.e., the percolation threshold; e.g., Rust and Cashman, 2011; Gonnermann et al., 2017; Giachetti et al., 2019). The magma may then either fragment around this porosity and continues its ascent as a mixture of gas and porous pyroclasts if the decompression is relatively high (e.g. Sparks, 1978; Papale, 1999; Rust and Cashman, 2011; Gonnermann et al., 2017, Fig. 5a), or reach the surface without fragmenting and produce a rhyolitic flow/dome if the decompression is relatively low (e.g. Taylor et al., 1983; Eichelberger et al., 1986; Newman et al., 1988, Fig. 5b). In both cases, above the percolation threshold, the magma/pyroclast is assumed to behave as an open system in terms of degassing.

We thus modified the model to assume that the magma behaves as a closed-system until its porosity reaches 65±5%, and then as an open system until the pyroclast/flow is quenched. The sensitivity of the model to the value of the percolation threshold is illustrated in Fig. A.1d. We used the solubility model of Liu et al. (2005) and the assumption of equilibrium degassing to calculate the porosity of the degassing magma in our model. Fig. 6 shows that most pyroclastic obsidians, obsidians from the flow, and degassed (i.e., dense, least rehydrated) porous pyroclasts can be fitted by some combination of closed- and open-system degassing. However, even taking into account the uncertainties associated with the initial δD and water content of the magma, the percolation threshold, and the water speciation model used (see sensitivity analysis in Appendix A), this simple model lacks of a process to explain some of the data, in particular the pyroclastic obsidians data with low H_2O content and relatively high δD.

In the next two sections, we discuss how the pyroclastic obsidians may acquire relatively high δD signatures compared to the degassing trend and examine the implications of two potential modes of formation for these samples.

6.2.2. Permeable foam collapse

The near absence of vesicles in both pyroclastic and flow obsidians combined with their relatively low water contents helped solidify acceptance of the ‘permeable foam collapse model’. In this model, slowly ascending magma becomes permeable, allowing gases to flow and escape, and then partly collapses to form

Please cite this article in press as: Giachetti, T., et al. D/H ratios and H_2O contents record degassing and rehydration history of rhyolitic magma and pyroclasts. Earth Planet. Sci. Lett. (2019), https://doi.org/10.1016/j.epsl.2019.115909

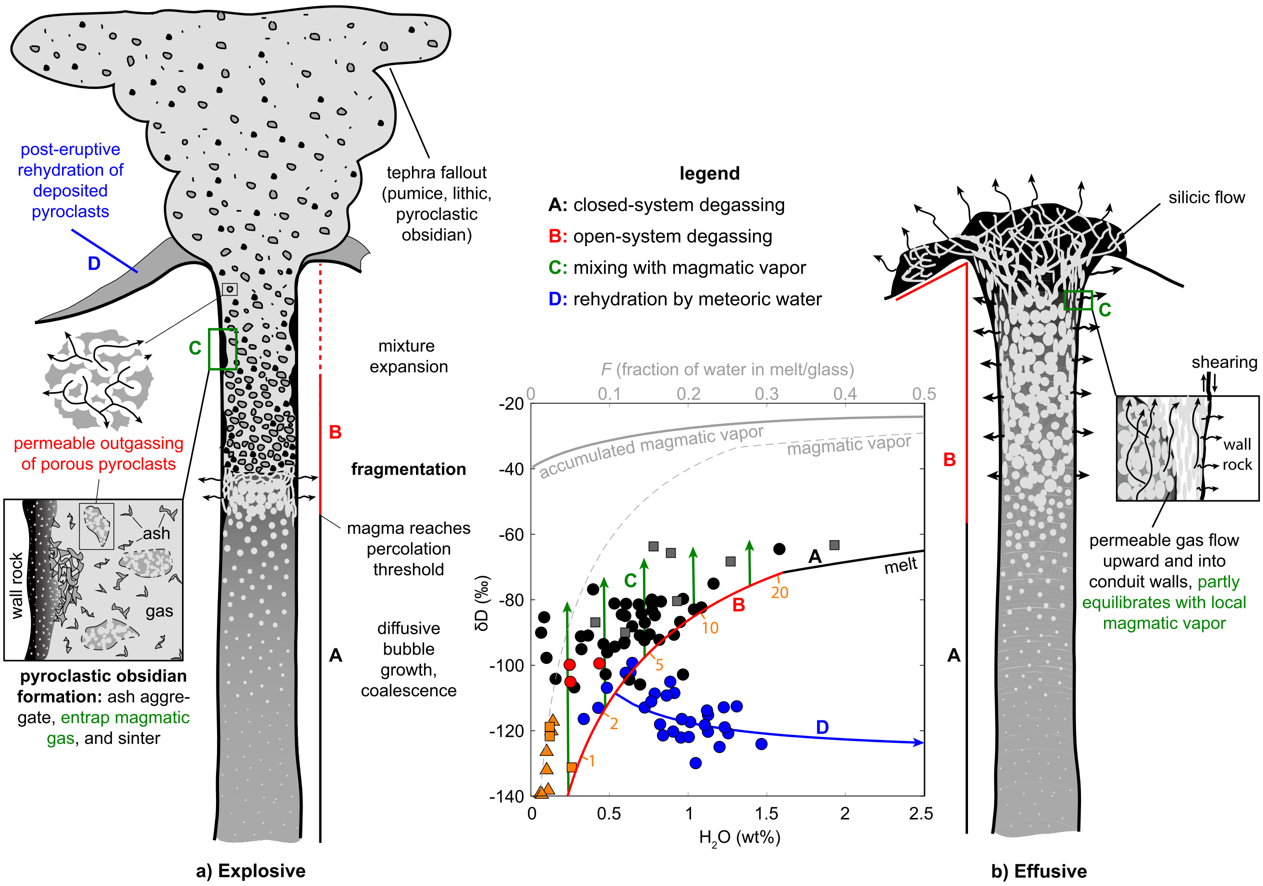

Fig. 5. Schematic diagram illustrating the different degassing processes taking place inside and outside the conduit during and after each phase of the eruption (see text for explanation). Curves A, B and D result from numerical modeling. A and B were obtained with an initial magmatic water content, H_2O_i, of 6 wt%, initial $\delta D = -49‰$, and a percolation threshold, ϕ_{cr}, of 65%, which fits most of the pyroclastic obsidians with a low δD and the most degassed (and dense) pumices that were very poorly rehydrated. C curves show mixing between particles and isotopically heavier magmatic water vapor either a) at different locations above the fragmentation level in the case of an explosive sub-Plinian phase, or b) within the degassed plug in the case of an effusive phase. Confining pressure is indicated in MPa using orange ticks along the degassing trend.

a vesicle-poor melt (Taylor et al., 1983; Eichelberger et al., 1986; Newman et al., 1988; Taylor, 1991; Jaupart and Allègre, 1991). This mechanism occurs when the ascending magma is either injected as dikes or into wall rock fractures, remains confined to the conduit walls where it is sheared, or forms a degassed plug at the top of the magmatic column (e.g., Taylor et al., 1983; Newman et al., 1988; Gonnermann and Manga, 2003; Rust et al., 2004; Rust and Cashman, 2007). During the slow ascent of the permeable magma, isotopically heavier magmatic vapor coming from the deeper degassing magma is continuously being fluxed through the network of interconnected vesicles and fractures, interacting with the melt (Fig. 5b). Because of its slow ascent rate, the magma is at equilibrium with the confining pressure and this interaction with the isotopically heavier magmatic vapor leads to an increase in the δD of the melt without any significant increase in its H_2O content (arrows labelled C on Fig. 5).

The graph on Fig. 5 shows that the H_2O content and δD measured in the Glass Mountain pyroclastic obsidians are consistent with this model: a slowly ascending magma behaves as a closed system before its porosity reaches the percolation threshold (trend labelled A), beyond which it degasses in open-system (B) and interacts with the isotopically heavy magmatic vapor (C), until fragments of this magma are broken at different depths, entrained, rapidly quenched, and deposited together with the porous tephra during a subsequent explosive phase of the eruption, forming pyroclastic obsidians. This mode of formation of the pyroclastic obsidians accounts for both 1) the wide range of water contents of ~1.5 wt%, due to the range of depths over which the degassed magma is being sampled by the explosive phase, and 2) the variability in δD of ~30‰, due to different extent of interaction with the isotopically light magmatic vapor. If the pyroclastic obsidians were formed by permeable foam collapse during the Glass Mountain eruption, the deepest sample was extracted from a confining pressure of about 20 MPa, while most of the pyroclastic obsidians were confined at pressured of 1-7 MPa, corresponding to a depth of 40-300 m assuming a completely dense plug (values calculated using the measured water contents, a temperature of 850 °C, the solubility model of Liu et al., 2005, and a plug density of 2360 kg m^{-3}). Formation of pyroclastic obsidians via foam collapse requires both the collapse of the foam, which would mostly occur during more effusive phase(s) of the eruption, and the destruction of the plug/dome during a subsequent explosive sequence. If the ascent rate is low enough to allow efficient magma outgassing and prevent fragmentation, the magma reaches the surface forming an obsidian flow/dome, with an on-average lower water content and δD than the pyroclastic obsidians (Fig. 5).

6.2.3. *Post-fragmentation ash sintering*

Based on the textures and volatiles contents of pyroclastic obsidians from Mono Craters, California, Gardner et al. (2017) and Watkins et al. (2017) recently questioned the precept that all pyroclastic obsidians formed by permeable foam collapse. Instead, they propose that some pyroclastic obsidians are created syn-explosively through multiple cycles of sintering of ash particles

Please cite this article in press as: Giachetti, T., et al. D/H ratios and H_2O contents record degassing and rehydration history of rhyolitic magma and pyroclasts. Earth Planet. Sci. Lett. (2019), https://doi.org/10.1016/j.epsl.2019.115909

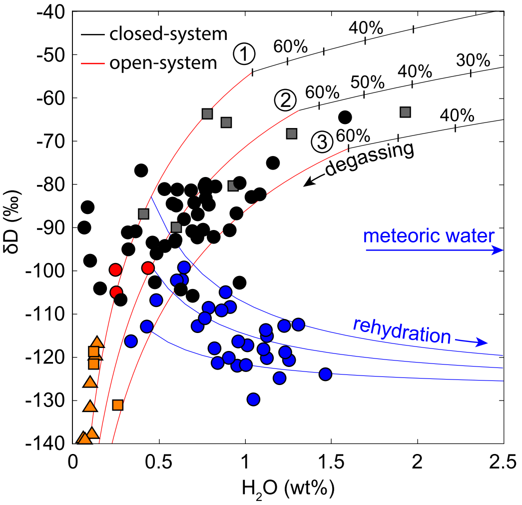

Fig. 6. Numerical models combining closed- and open-system degassing. The initial magma degasses in closed-system (black lines) until its porosity, marked by vertical black ticks, reaches 65±5% and becomes permeable. It then degasses in open-system (red lines) until sample final quench. Three cases covering the uncertainties associated with initial conditions and percolation threshold are taken into account: an initial magmatic water content, H_2O_i, of 4 wt%, initial $\delta D = -30‰$, and a percolation threshold, ϕ_{cr}, of 70% (case 1), $H_2O_i = 5$ wt%, $\delta D = -40‰$, $\phi_{cr} = 65\%$ (case 2), and $H_2O_i = 6$ wt%, $\delta D = -50‰$, $\phi_{cr} = 60\%$ (case 3). Porous pyroclasts have a water content of about 0.45 wt% immediately after the eruption and before rehydration and a δD of −115‰ to −83‰ depending of the scenario considered. During rehydration, meteoric water with a δD of −95‰ slowly diffuses into the matrix glass for about a thousand years before sample collection and analysis, slowly increasing H_2O and decreasing δD. Sample symbols are identical to those in Fig. 2. See also Appendix A for sensitivity analysis of this model. (For interpretation of the colors in the figure(s), the reader is referred to the web version of this article.)

along conduit walls, and fracturing back into the eruptive column, all above the level of fragmentation (Gardner et al., 2017; Watkins et al., 2017). During this process of formation of the pyroclastic obsidians, magmatic gas from the conduit is entrapped in between individual grains (Fig. 5a), and because of the relatively rapid sintering of the ash particles that isolate individual pores (a few tens to few hundreds seconds, Gardner et al., 2018), ash and entrapped gas partly equilibrate in closed system. As for the permeable foam collapse model, this leads to an increase in δD of the ash without any significant increase in H_2O (arrows labelled C on Fig. 5), and pyroclastic obsidians formation by post-fragmentation ash sintering on the conduit sides can also account for the wide range of δD observed at a given H_2O_t content.

Assuming the pyroclastic obsidians analyzed in this study formed by ash sintering, this occurred solely during the first, explosive phase of the eruption that also produced the porous pyroclasts. In this case, the pyroclastic obsidian with the highest water content (1.58 wt%) thus records a minimum pressure for the fragmentation level (∼20 MPa). This pressure is consistent with the fact that magma becomes permeable around 15-20 MPa (i.e., at a porosity of 60-70%) and that fragmentation is thought to occur slightly below this pressure (Rust and Cashman, 2011). Most pyroclastic obsidians have water contents around 0.5-0.7 wt% and speciation data obtained by FTIR indicate that such samples equilibrated with a water vapor phase at temperatures of 420-635 °C (Table 2), which is close to or below the expected glass transition temperature at these measured water contents (580-610 °C, Deubener et al., 2003). Using these temperatures, the solubility model of Liu et al. (2005) suggests that these pyroclastic obsidians equilibrate at pressures of 1-2.2 MPa, that is well above the fragmentation level calculated using the water-rich pyroclastic obsidian, consistent with the model of Gardner et al. (2017) and Watkins et al. (2017).

7. Conclusions

Volcanic eruptions of rhyolitic magma commonly show shifts from a powerful explosive episode to a more gentle effusive phase during which obsidian flows/domes form, causing problems in terms of hazards assessment and mitigation. The presence of juvenile obsidian pyroclasts throughout the tephra from the explosive phase is another characteristic of rhyolitic eruptions. However, their mechanism of formation and the information they can provide in terms of syn-eruptive magma degassing are still the object of active research. In this study, the rhyolitic juvenile components of both the explosive and effusive products from the 1060CE Glass Mountain eruption of Medicine Lake Volcano were analyzed for their porosity, water content, and hydrogen isotopic ratio. These data were compared with numerical models of syn-eruptive magma degassing carried out assuming different scenarios of magma ascent in the conduit (in closed-system, open-system, or a combination thereof), and model of post-eruptive matrix glass rehydration.

Water contents and isotopic ratios measured in porous pyroclasts are affected by post-eruptive matrix glass rehydration as shown both by the negative relationship between water content and δD, and by the positive correlation between water content and sample porosity. These relationships are satisfactorily fitted by numerical models suggesting that all porous pyroclasts had a magmatic water content close to 0.45 wt% immediately after the eruption, and that water diffused into the matrix glass of these porous pyroclasts at an average rate of $10^{-23.5\pm0.5}$ $m^2\,s^{-1}$ during the ∼960 years between the eruption and sample analysis. Due to the absence of open pores in pyroclastic and flow obsidians, these samples are not affected by rehydration.

Measured water contents and δD values in all samples are consistent with the syn-eruptive degassing of a rhyolitic magma initially containing 5±1 wt% of water with a δD of −40±10‰. During its ascent towards the surface, magma degasses in closed-system until its porosity reaches a value of about 65±5% (corresponding to a confining pressure of 15-20 MPa), beyond which degassing occurs in open-system until sample quench. During the initial, explosive phase of the eruption, the rapidly ascending magma fragments soon after it reaches a permeable state, creating porous pyroclasts and ash that continue to degas in open-system within an expanding magmatic gas phase down to a value of about 0.45 wt% H_2O.

As suggested by recent studies, some of the ash may aggregate and sinter on the conduit sides at different depths above the fragmentation level, partly equilibrating with the local magmatic vapor, which would explain both the wide range of H_2O contents and the high variability in δD measured in the pyroclastic obsidians. Using only H_2O contents and δD values, it is impossible to rule out the possibility that pyroclastic obsidians may also form by permeable foam collapse either near the conduit sides during the explosive phase itself, or during more effusive periods in between explosive events (vanguard magma). Further detailed work on the texture and volatile composition of the pyroclastic obsidians throughout the eruptive sequence is necessary to discriminate the two modes of formation. During the final effusive phase of the eruption, the slowly ascending magma degasses in open-system in the shallowest part of the conduit and partly interacts with the isotopically heavier magmatic vapor continuously/repeatedly flowing through the network of interconnected pores and fractures, until it collapses and reaches the surface, creating flow obsidians with low H_2O content and δD.

Unless a careful assessment of post-eruptive rehydration is first carried out, this study shows that H_2O measured in porous pyroclasts of a few hundred years or more cannot be reliably used to infer the extent of syn-eruptive magma degassing. Provided their

Please cite this article in press as: Giachetti, T., et al. D/H ratios and H_2O contents record degassing and rehydration history of rhyolitic magma and pyroclasts. Earth Planet. Sci. Lett. (2019), https://doi.org/10.1016/j.epsl.2019.115909

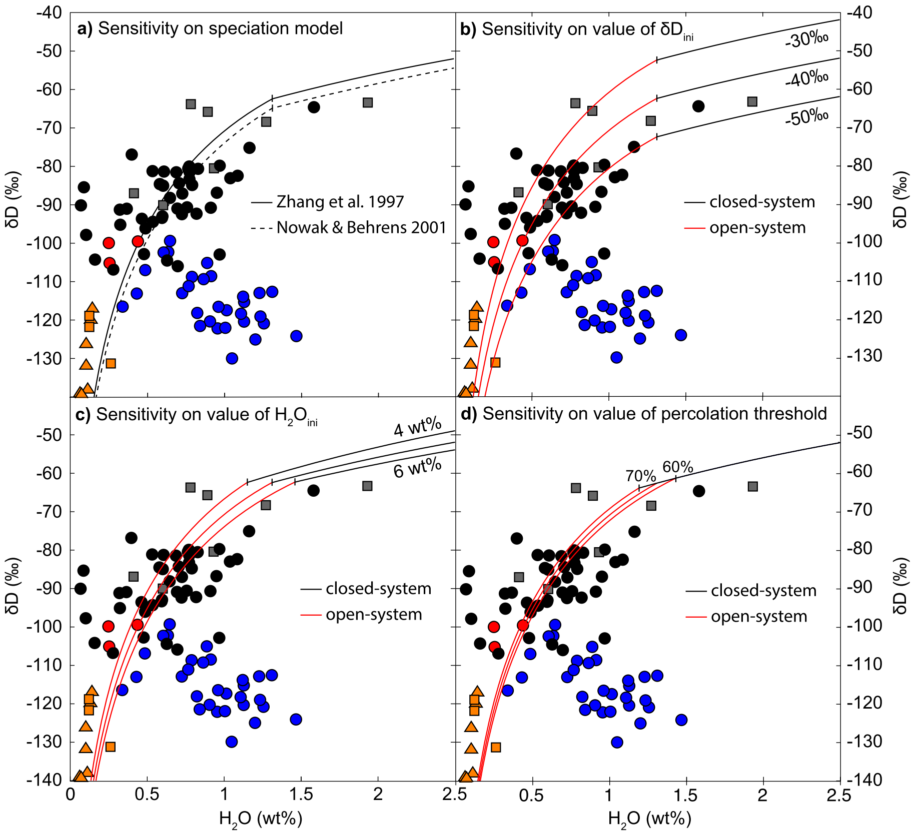

Fig. A.1. Sensitivity of the degassing model to **a)** the speciation model used (i.e., Zhang et al. (1997) or Nowak and Behrens (2001)), **b)** the initial δD (−30‰, −40‰, and −50‰), **c)** the initial water content (4 wt%, 5 wt%, and 6 wt%), and **d)** the value of the percolation threshold (60%, 65%, and 70%). In the speciation model of Nowak and Behrens (2001), the equilibrium constant of the speciation reaction is given by $K = 27.98 \times e^{-4210/T}$, with T in Kelvin. The reference model is performed with H_2O_{ini} = 5 wt%, $\delta D_{ini} = -40$‰, and a percolation threshold of 65%.

formation mechanism can be better understand, detailed analysis of the variations in texture and volatile content of pyroclastic obsidians throughout the explosive phase will help placing constraints on the depth of the fragmentation level (and its variation during the eruption) and/or the thickness of a degassed plug during more effusive phases of rhyolitic eruptions. This would help finding the cause(s) of the common shifts in eruptive style observed during rhyolitic eruptions.

Declaration of competing interest

The authors declare that they have no known competing financial interests or personal relationships that could have appeared to influence the work reported in this paper.

Acknowledgements

The authors would like to thank Jim Palandri who ran some of the TC/EA analyses and Jim Gardner, Jim Watkins and Julie Donnelly-Nolan for their discussions. TG and TS are grateful to Helge Gonnermann who facilitated the field work carried out at Medicine Lake. The paper greatly benefited from the thorough reviews of Mike Cassidy, an anonymous reviewer and Editor Tamsin Mather. TG was partly supported by the National Science Foundation grant EAR-1725207, and INB and MRH were supported by grant EAR-1822977. Any opinions, findings, and conclusions or recommendations expressed in this material are those of the authors and do not necessarily reflect the views of the National Science Foundation.

Appendix A. Sensitivity analysis

Fig. A.1 illustrates the sensitivity of the degassing model to the value of the percolation threshold (i.e., the porosity at which the magma becomes permeable and allow for degassing in open system), the initial water content, the initial δD, and the speciation model used. It shows that the values of the initial δD has the highest impact on the model.

Appendix B. Supplementary material

Supplementary material related to this article can be found online at https://doi.org/10.1016/j.epsl.2019.115909.

References

Anderson, C.A., 1933. Volcanic history of Glass Mountain, northern California. Am. J. Sci. 5 (26), 485–506.

Anovitz, L.M., Cole, D.R., Riciputi, L.R., 2009. Low-temperature isotopic exchange in obsidian: implications for diffusive mechanisms. Geochim. Cosmochim. Acta 73 (13), 3795–3806.

Behrens, H., Tamic, N., Holtz, F., 2004. Determination of the molar absorption coefficient for the infrared absorption band of CO_2 in rhyolitic glasses. Am. Mineral. 89 (2–3), 301–306.

Bowen, G.J., Wassenaar, L.I., Hobson, K.A., 2005. Global application of stable hydrogen and oxygen isotopes to wildlife forensics. Oecologia 143 (3), 337–348.

Bursik, M., 1993. Subplinian eruption mechanisms inferred from volatile and clast dispersal data. J. Volcanol. Geotherm. Res. 57 (1–2), 57–70.

Cabrera, A., Weinberg, R.F., Wright, H.M., Zlotnik, S., Cas, R.A., 2011. Melt fracturing and healing: a mechanism for degassing and origin of silicic obsidian. Geology 39 (1), 67–70.

Castro, J.M., Dingwell, D.B., 2009. Rapid ascent of rhyolitic magma at Chaitén volcano, Chile. Nature 461 (7265), 780.

Please cite this article in press as: Giachetti, T., et al. D/H ratios and H_2O contents record degassing and rehydration history of rhyolitic magma and pyroclasts. Earth Planet. Sci. Lett. (2019), https://doi.org/10.1016/j.epsl.2019.115909

Castro, J.M., Schipper, C.I., Mueller, S.P., Militzer, A., Amigo, A., Parejas, C.S., Jacob, D., 2013. Storage and eruption of near-liquidus rhyolite magma at Cordón Caulle, Chile. Bull. Volcanol. 75 (4), 702.

Castro, J.M., Bindeman, I.N., Tuffen, H., Schipper, C.I., 2014. Explosive origin of silicic lava: textural and δD-H_2O evidence for pyroclastic degassing during rhyolite effusion. Earth Planet. Sci. Lett. 405, 52–61.

Davisson, M., Rose, T., 1997. Comparative Isotope Hydrology Study of Groundwater Sources and Transport in the Three Cascade Volcanoes of Northern California. Tech. rep. Lawrence Livermore National Lab. (LLNL), Livermore, CA, United States.

DeGroat-Nelson, P.J., Cameron, B.I., Fink, J.H., Holloway, J.R., 2001. Hydrogen isotope analysis of rehydrated silicic lavas: implications for eruption mechanisms. Earth Planet. Sci. Lett. 185, 331–341.

Deubener, J., Muller, R., Behrens, H., Heide, G., 2003. Water and the glass transition temperature of silicate melts. Non-Cryst. Solids 330, 268–273.

Dobson, P.F., Epstein, S., Stolper, E.M., 1989. Hydrogen isotope fractionation between coexisting vapor and silicate glasses and melts at low pressure. Geochim. Cosmochim. Acta 53 (10), 2723–2730.

Donnelly-Nolan, J., Nathenson, M., Champion, D.E., Ramsey, D.W., Lowenstern, J.B., Ewert, J.W., 2007. Volcano Hazards Assessment for Medicine Lake Volcano, Northern California. USGS-Scientific Investigation Report 5174-A.

Donnelly-Nolan, J.M., Champion, D.E., Miller, C.D., Grove, T.L., Trimble, D.A., 1990. Post-11,000-year volcanism at Medicine Lake Volcano, cascade range, northern California. J. Geophys. Res. 95, 19,693–19,704.

Donnelly-Nolan, J.M., Grove, T.L., Lanphere, M.A., Champion, D.E., Ramsey, D.W., 2008. Eruptive history and tectonic setting of Medicine Lake Volcano, a large rear-arc volcano in the southern Cascades. J. Volcanol. Geotherm. Res. 177, 313–328.

Eichelberger, J.C., Carrigan, C.R., Westrich, H.R., Price, R.H., 1986. Non-explosive silicic volcanism. Nature 323, 598–602.

Friedman, I., Long, W., 1976. Hydration rate of obsidian. Science 191, 347–352.

Friedman, I., Smith, R., 1958. The deuterium content of water in some volcanic glasses. Geochim. Cosmochim. Acta 15, 218–228.

Friedman, I., Smith, R.L., 1960. Part i, the development of the method. Am. Antiq. 25 (4), 476–493.

Friedman, I., Gleason, J., Sheppard, R.A., Gude 3rd, A.J., 1993. Deuterium Fractionation as Water Diffuses into Silicic Volcanic Ash. American Geophysical Union Geophysical Monograph Series, vol. 78, pp. 321–323.

Gardner, J.E., Llewellin, E.W., Watkins, J.M., Befus, K.S., 2017. Formation of obsidian pyroclasts by sintering of ash particles in the volcanic conduit. Earth Planet. Sci. Lett. 459, 252–263.

Gardner, J.E., Wadsworth, F.B., Llewellin, E.W., Watkins, J.M., Coumans, J.P., 2018. Experimental sintering of ash at conduit conditions and implications for the longevity of tuffisites. Bull. Volcanol. 80 (3), 23.

Gerlach, T.M., Westrich, H.R., Symonds, R.B., 1996. Pre-eruption vapor in magma of the climactic Mount Pinatubo eruption: source of the giant stratospheric sulfur dioxide cloud. In: Newhall, C.G., Punongbayan, R. (Eds.), Fire and Mud: Eruptions and Lahars of Mount Pinatubo, Philippines. University of Washington Press, Seattle, pp. 415–433.

Giachetti, T., Gonnermann, H.M., 2013. Water in volcanic pyroclast: rehydration or incomplete degassing? Earth Planet. Sci. Lett. 369–370, 317–332.

Giachetti, T., Druitt, T.H., Burgisser, A., Arbaret, L., Galven, C., 2010. Bubble nucleation, growth and coalescence during the 1997 Vulcanian explosions of Soufrière Hills Volcano, Montserrat. J. Volcanol. Geotherm. Res. 193 (3), 215–231.

Giachetti, T., Gonnermann, H.M., Gardner, J.E., Shea, T., Gouldstone, A., 2015. Discriminating secondary from magmatic water in rhyolitic matrix-glass of volcanic pyroclasts using thermogravimetric analysis. Geochim. Cosmochim. Acta 148, 457–476.

Giachetti, T., Gonnermann, H.M., Gardner, J.E., Burgisser, A., Hajimirza, S., Earley, T.C., Truong, N., Toledo, P., 2019. Bubble coalescence and percolation threshold in expanding rhyolitic magma. Geochem. Geophys. Geosyst. 20 (2), 1054–1074.

Gonnermann, H.M., Manga, M., 2003. Explosive volcanism may not be an inevitable consequence of magma fragmentation. Nature 426, 432–435.

Gonnermann, H.M., Giachetti, T., Fliedner, C., Nguyen, C.T., Houghton, B.F., Crozier, J.A., Carey, R.J., 2017. Permeability during magma expansion and compaction: observations and experiments. J. Geophys. Res., Solid Earth 122.

Grove, T.L., Donnelly-Nolan, J.M., 1986. The evolution of young silicic lavas at Medicine Lake Volcano, California: implications for the origin of compositional gaps in calc-alkaline series lavas. Contrib. Mineral. Petrol. 92, 281–302.

Grove, T.L., Donnelly-Nolan, J.M., Housh, T., 1997. Magmatic processes that generated the rhyolite of Glass Mountain, Medicine Lake Volcano, N. California. Contrib. Mineral. Petrol. 127, 205–223.

Harford, C., Sparks, R., Fallick, A., 2003. Degassing at the Soufrière Hills Volcano, Montserrat, recorded in matrix glass compositions. J. Petrol. 44 (8), 1503–1523.

Heiken, G., 1978. Plinian-type eruptions in the Medicine Lake Highland, California, and the nature of the underlying magma. J. Volcanol. Geotherm. Res. 4, 375–402.

Hildreth, W., Fierstein, J., 2012. The Novarupta-Katmai eruption of 1912? Largest eruption of the twentieth century. Centennial Perspectives: U.S. Geological Survey Professional Paper 1791, 278 pp.

Houghton, B.F., Wilson, C.J.N., 1989. A vesicularity index for pyroclastic deposits. Bull. Volcanol. 51, 451–462.

Hudak, M.R., Bindeman, I.N., 2018. Conditions of pinnacle formation and glass hydration in cooling ignimbrite sheets from H and O isotope systematics at Crater Lake and the Valley of Ten Thousand Smokes. Earth Planet. Sci. Lett. 500, 56–66.

Hui, H., Zhang, Y., Xu, Z., Behrens, H., 2008. Pressure dependence of the speciation of dissolved water in rhyolitic melts. Geochim. Cosmochim. Acta 72, 3229–3240.

Jaupart, C., Allègre, C.J., 1991. Gas content, eruption rate and instabilities of eruption regime in silicic volcanoes. Earth Planet. Sci. Lett. 102, 413–429.

Kusakabe, M., Sato, H., Nakada, S., Kitamura, T., 1999. Water contents and hydrogen isotopic ratios of rocks and minerals from the 1991 eruption of Unzen volcano, Japan. J. Volcanol. Geotherm. Res. 89 (1–4), 231–242.

Lara, L.E., 2009. The 2008 eruption of the Chaitén volcano, Chile: a preliminary report. Andean Geol. 36 (1).

Liritzis, I., Laskaris, M., 2011. Fifty years of obsidian hydration dating in archaeology. J. Non-Cryst. Solids 357, 2011–2023.

Liritzis, I., Diakostamatiou, M., Stevenson, C., Novak, S., Abdelrehim, I., 2004. Dating of hydrated obsidian surfaces by sims-ss. J. Radioanal. Nucl. Chem. 261 (1), 51–60.

Liu, Y., Zhang, Y., Behrens, H., 2005. Solubility of H_2O in rhyolitic melts at low pressures and a new empirical model for mixed H_2O-CO_2 solubility in rhyolitic melts. J. Volcanol. Geotherm. Res. 143, 219–235.

Mandeville, C.W., Webster, J.D., Tappen, C., Taylor, B.E., Timbal, A., Sasaki, A., Hauri, E., Bacon, C.R., 2009. Stable isotope and petrologic evidence for open-system degassing during the climactic and pre-climactic eruptions of Mt. Mazama, Crater Lake, Oregon. Geochim. Cosmochim. Acta 73 (10), 2978–3012.

Martin, E., Bindeman, I., Balan, E., Palandri, J., Seligman, A., Villemant, B., 2017. Hydrogen isotope determination by TC/EA technique in application to volcanic glass as a window into secondary hydration. J. Volcanol. Geotherm. Res. 348, 49–61.

McIntosh, I.M., Llewellin, E.W., Humphreys, M.C.S., Nichols, A.R.L., Burgisser, A., Schipper, C.I., Larsen, J.F., 2014. Distribution of dissolved water in magmatic glass records growth and resorption of bubbles. Earth Planet. Sci. Lett. 401, 1–11.

McIntosh, I.M., Nichols, A.R., Tani, K., Llewellin, E.W., 2017. Accounting for the species-dependence of the 3500 cm^{-1} H_2O_t infrared molar absorptivity coefficient: implications for hydrated volcanic glasses. Am. Mineral., J. Earth Planet. Mater. 102 (8), 1677–1689.

Mitchell, S.J., McIntosh, I.M., Houghton, B.F., Carey, R.J., Shea, T., 2018. Dynamics of a powerful deep submarine eruption recorded in H_2O contents and speciation in rhyolitic glass: the 2012 Havre eruption. Earth Planet. Sci. Lett. 494, 135–147.

Newman, S., Stolper, E.M., Epstein, S., 1986. Measurement of water in rhyolitic glasses: calibration of an infrared spectroscopic technique. Am. Mineral. 71, 1527–1541.

Newman, S., Epstein, S., Stolper, E., 1988. Water, carbon dioxide, and hydrogen isotopes in glasses from the ca. 1340 ad eruption of the Mono Craters, California: constraints on degassing phenomena and initial volatile content. J. Volcanol. Geotherm. Res. 35 (1–2), 75–96.

Nowak, M., Behrens, H., 2001. Water in rhyolitic magmas: getting a grip on a slippery problem. Earth Planet. Sci. Lett. 184 (2), 515–522.

Papale, P., 1999. Strain-induced magma fragmentation in explosive eruptions. Nature 397 (6718), 425.

Qi, H., Coplen, T.B., Gehre, M., Vennemann, T.W., Brand, W.A., Geilmann, H., Olack, G., Bindeman, I.N., Palandri, J., Huang, L., et al., 2017. New biotite and muscovite isotopic reference materials, USGS57 and USGS58, for δ^2H measurements–a replacement for NBS 30. Chem. Geol. 467, 89–99.

Rempel, A.W., Bindeman, I.N., 2019. A model for the development of stable isotopic water signatures of tephra deposited on ice following subglacial caldera collapse. J. Volcanol. Geotherm. Res. 377, 131–145.

Ross, C., Smith, R., 1955. Water and other volatiles in volcanic glasses. Am. Mineral. 40, 1071–1089.

Rust, A., Cashman, K., 2007. Multiple origins of obsidian pyroclasts and implications for changes in the dynamics of the 1300 bp eruption of Newberry Volcano, USA. Bull. Volcanol. 69 (8), 825–845.

Rust, A., Cashman, K.V., Wallace, P.J., 2004. Magma degassing buffered by vapor flow through brecciated conduit margins. Geology 32, 349–352.

Rust, A.C., Cashman, K.V., 2011. Permeability controls on expansion and size distributions of pyroclasts. J. Geophys. Res. 116, B11202.

Schipper, C.I., Castro, J.M., Tuffen, H., James, M.R., How, P., 2013. Shallow vent architecture during hybrid explosive-effusive activity at Cordón Caulle (Chile, 2011–12): evidence from direct observations and pyroclast textures. J. Volcanol. Geotherm. Res. 262, 25–37.

Seligman, A.N., Bindeman, I.N., Watkins, J.M., Ross, A.M., 2016. Water in volcanic glass: from volcanic degassing to secondary hydration. Geochim. Cosmochim. Acta 191, 216–238.

Shea, T., Houghton, B.F., Gurioli, L., Cashman, K.V., Hammer, J.E., Hobden, B.J., 2010. Textural studies of vesicles in volcanic rocks: an integrated methodology. J. Volcanol. Geotherm. Res. 190, 270–289.

Silva Parejas, C., Lara, L., Bertin, D., Amigo, A., Orozco, G., 2012. The 2011-2012 eruption of Cordón Caulle volcano (Southern Andes): evolution, crisis management and current hazards. In: EGU General Assembly Conference Abstracts, vol. 14, p. 9382.

Please cite this article in press as: Giachetti, T., et al. D/H ratios and H_2O contents record degassing and rehydration history of rhyolitic magma and pyroclasts. Earth Planet. Sci. Lett. (2019), https://doi.org/10.1016/j.epsl.2019.115909

Sparks, R.S.J., 1978. The dynamics of bubble formation and growth in magmas. J. Volcanol. Geotherm. Res. 3, 1–37.

Stasiuk, M.V., Barclay, J., Carroll, M.R., Jaupart, C., Ratté, J.C., Sparks, R.S.J., Tait, S.R., 1996. Degassing during magma ascent in the Mule Creek vent (USA). Bull. Volcanol. 58 (2–3), 117–130.

Stevenson, R.J., Dingwell, D.B., Webb, S.L., Sharp, T.G., 1996. Viscosity of microlite-bearing rhyolitic obsidians: an experimental study. Bull. Volcanol. 58, 298–309.

Stolper, E., 1982. Water in silicate glasses: an infrared spectroscopic study. Contrib. Mineral. Petrol. 81, 1–17.

Tatlock, D.B., Flanagan, F.J., Bastron, H., Berman, S., Sutton Jr., A.L., 1976. Rhyolite, RGM-1, from Glass Mountain, California. In: Descriptions and Analyses of Eight New USGS Rock Standards. U.S. Geol. Surv., Prof. Pap., pp. 11–14.

Taylor, B., 1991. Degassing of Obsidian Dome rhyolite, Inyo volcanic chain, California. In: Stable Isotope Geochemistry: A Tribute to Samuel Epstein. In: Geochem. Soc. Spec. Publ., vol. 3, pp. 339–353.

Taylor, B.E., Eichelberger, J., Westrich, H., 1983. Hydrogen isotopic evidence of rhyolitic magma degassing during shallow intrusion and eruption. Nature 306 (5943), 541.

Taylor, H.P., 1986. Igneous rocks ii: isotopic case studies of circum pacific magmatism. In: Stables Isotopes in High Temperature. Geological Processes.

Tuffen, H., Dingwell, D.B., Pinkerton, H., 2003. Repeated fracture and healing of silicic magma generate flow banding and earthquakes? Geology 31 (12), 1089–1092.

Tuffen, H., Owen, J., Denton, J., 2010. Magma degassing during subglacial eruptions and its use to reconstruct palaeo-ice thicknesses. Earth-Sci. Rev. 99 (1–2), 1–18.

Waters, L.E., Lange, R.A., 2016. No effect of H_2O degassing on the oxidation state of magmatic liquids. Earth Planet. Sci. Lett. 447, 48–59.

Watkins, J., Gardner, J., Befus, K., 2017. Nonequilibrium degassing, regassing, and vapor fluxing in magmatic feeder systems. Geology 45 (2), 183–186.

Watkins, J.M., Manga, M., DePaolo, D.J., 2012. Bubble geobarometry: a record of pressure changes, degassing, and regassing at Mono Craters, California. Geology 40, 699–702.

Zhang, Y., 1999. A criterion for the fragmentation of bubbly magma based on brittle failure theory. Nature 402, 648–650.

Zhang, Y., Ni, H., 2010. Diffusion of H, C, and O components in silicate melts. Rev. Mineral. Geochem. 72, 171–225.

Zhang, Y., Jenkins, J., Xu, Z., 1997. Kinetics of the reaction $H_2O + O \leftrightharpoons 2OH$ in rhyolitic glasses upon cooling: geospeedometry and comparison with glass transition. Geochim. Cosmochim. Acta 61 (11), 2167–2173.

Please cite this article in press as: Giachetti, T., et al. D/H ratios and H_2O contents record degassing and rehydration history of rhyolitic magma and pyroclasts. Earth Planet. Sci. Lett. (2019), https://doi.org/10.1016/j.epsl.2019.115909